Journal of Applied Geophysics 73 (2011) 93–100

Contents lists available at ScienceDirect

Journal of Applied Geophysics

journal homepage: www.elsevier.com/locate/jappgeo

AVA seismic reflectivity analysis in carbon dioxide accumulations: Sensitivity to CO_2 phase and saturation

Claudia L. Ravazzoli *, Julián L. Gómez

CONICET and Facultad de Ciencias Astronómicas y Geofísicas, Universidad Nacional de La Plata, Paseo del Bosque S/N, B1900FWA, La Plata, Argentina

ARTICLE INFO

Article history:
Received 30 September 2009
Accepted 24 November 2010
Available online 2 December 2010

Keywords:
CO_2 sequestration
Seismic monitoring
AVO
Solubility
Partial saturation

ABSTRACT

Seismic monitoring of sequestered carbon dioxide (CO_2) in underground deposits is a matter of growing importance. The subsurface monitoring of this greenhouse gas is possible due to the marked contrast between the physical properties of natural reservoir fluids and those of carbon dioxide after the injection. This technique makes necessary the investigation of appropriate seismic indicators to link seismic attributes to petrophysical properties, composition and state of the rock as well as pore-fluid type and *in-situ* physical conditions. With this motivation in mind, we use a Biot–Gassmann formulation to model the theoretical P-wave amplitude reflection coefficients vs. angle of incidence in the seismic range when a planar P-wave strikes the interface between a caprock and a porous sandstone which has its pore space saturated by a mixture of CO_2 with brine or oil at different states (supercritical, liquid and gas). The effects of dissolution of CO_2 in oil and the existence of a saturation threshold, above which a free CO_2 phase develops, are included in the computations. Attention is particularly focused on the sensitivity of the classic best-fit amplitude variations with angle coefficients, to different degrees of CO_2 saturation. We conclude from this analysis that the changes in seismic AVA attributes between 30 and 40 degrees can be useful to infer bounds on the CO_2 saturation degree, to detect the presence of immiscible CO_2 phase and, in some cases, to infer the physical state of the accumulations.

1. Introduction

Carbon dioxide is released into our atmosphere during hydrocarbon production and mainly when carbon-containing fossil fuels such as oil, natural gas, and coal are burned during combustion. As a result of the world-wide consumption of such fossil fuels, the amount of CO_2 in the atmosphere has largely increased over the past century. It is now widely accepted that the continued increase in CO_2 concentration is a major agent in global climate change (Metz et al., 2005).

Many carbon dioxide capture and storage projects are being developed worldwide to reduce the emission of greenhouse gases in the atmosphere as a way to mitigate climate changes in a transition period towards the use of more sustainable energies, in accordance with the objectives of Kyoto agreement. The sequestration and geological storage of CO_2 in many cases is a feasible option to accomplish this goal, giving rise to the science of CO_2 sequestration, a new challenge for governments, scientists and engineers (Raistrick, 2008). However this practice requires a careful surveillance to prevent this greenhouse gas from seeping back to the atmosphere or into fresh water aquifers.

In most cases, the appreciable contrast between the physical properties of natural reservoir fluids and those of carbon dioxide allows the utilization of 4D seismic methods as a monitoring tool of the spatial and temporal evolution of this substance after the injection. Very good illustrations of this technique are described by Arts et al. (2004), Chadwick et al. (2005) and Arts et al. (2007) at Sleipner injection field (North Sea, Norway), among other works. In addition, identification of supercritical CO_2 in 3D seismic surveys has been reported (Purcell et al., 2010). While it is accepted that 4D seismic methods are able to monitor the presence or absence of CO_2, their ability to quantify the saturation and state of this fluid within the reservoir is still under discussion. This makes it necessary to search for reliable seismic indicators for CO_2 saturated geological formations.

It is widely recognized that the dependence of seismic reflection amplitude vs. offset from source to receiver (AVO) or equivalently, amplitude variations with ray angle (AVA) are important tools for reservoir lithology and fluid characterization (Avseth et al., 2005; Castagna and Backus, 1993). With this idea, Brown et al. (2007) suggested an AVO based method to monitor both presence and degree of CO_2 saturation. They showed that variations in the best-fitting AVO parameters before and after CO_2 injection may be seismically noticeable. More recently, Hardage and Silva (2009) presented an AVO model in brine reservoirs oriented to the identification of CO_2-brine interfaces. However, none of these authors take into account the high variability of the many parameters and state variables involved

* Corresponding author. Tel.: +54 2214536593; fax: +54 2214536591.
E-mail addresses: claudia@fcaglp.fcaglp.unlp.edu.ar (C.L. Ravazzoli), jgomez@fcaglp.fcaglp.unlp.edu.ar (J.L. Gómez).

0926-9851/$ – see front matter © 2010 Elsevier B.V. All rights reserved.
doi:10.1016/j.jappgeo.2010.11.010

in CO_2 sequestration problems. This led us to model the seismic P-wave reflection coefficient at the top of a layer containing mixtures of CO_2 and brine or oil, for variable saturation and different *in-situ* pore pressure and temperature conditions (e.g. in cold and warm basins). Moreover, taking into account that in oil reservoirs an important fraction of the CO_2 injected can be absorbed (which is the base of *solubility trapping* strategies), following the ideas presented by Carcione et al. (2006), we included these solubility effects in our computations. These results then allowed us to perform a parametric analysis on the corresponding AVO parameters.

From these experiments we conclude that the AVA intercept parameter shows a monotonic decreasing behavior, with very strong variations with respect to the pre-injection state and for low CO_2 saturation, showing slower changes at higher saturation. The gradient AVA parameter also decays substantially in the low CO_2 saturation range, being less sensitive than the intercept. The third AVO parameter (the curvature), related to the far offset information, is the less sensitive of the three, showing changes that in some cases may be well below the seismic resolution. With regards to the dissolution of CO_2 in oil reservoirs, our model estimates allow us to conclude that it would be possible to use time lapse seismic data to detect and monitor the free CO_2 phase, which forms after the oil is completely saturated.

These results suggest that, under certain conditions, seismic AVA parameters can be used not only to establish bounds on CO_2 saturation levels but also to characterize the physical state of this substance in subsurface accumulations and leakages at different depth levels.

2. Modeling procedure and main assumptions

The formulation and solution of the energy and amplitude splitting problem when a monochromatic plane compressional wave strikes obliquely at a plane interface between two isotropic porous saturated homogeneous half spaces was treated by different authors, such as Deresiewicz and Rice (1960), Dutta and Odé (1983), Santos et al. (1992) and Ravazzoli (2001). Following the ideas in those papers, in this work the mechanical behavior of the porous media is described in terms of the classic constitutive relations and equations of motion given by Biot (1956, 1962). At the interface, for both reflected and transmitted phases, two reflected compressional waves (fast and slow) and a shear wave are generated. However, it must be remarked that when a low frequency seismic wave propagates through a porous saturated medium, due to fluid viscosity both constituents (solid and fluid) move in phase, and consequently, the model response is equivalent to that resulting from the formulation given by Gassmann (1951). In this connection, since in this work we are interested in frequencies within the seismic range, we do not study slow wave conversions and focus in the fast P-wave reflection coefficient. Nevertheless, and only for selected cases, we also analyze the shear wave reflection coefficient.

In this work, it is assumed that the mixture of CO_2 and brine or CO_2 and reservoir oil at the pore scale can be treated as a viscous single phase effective fluid, as explained in the next section. The dissolution of a fraction of CO_2 and the presence of a remaining free part is taken into account in these computations, whose effect is particularly important for the case of CO_2 injected in oil reservoirs.

We also consider that the CO_2 is uniformly distributed within the pore space in one of the half spaces, forming a layer of thickness larger than the wavelengths of the incident waves. The computation of seismic reflection coefficients for the case of thin layers or spatially variable CO_2 distribution (such as patchy saturation) would require a more complex treatment.

In general, the presence of intrinsic dissipation in wave propagation models lead to a complex frequency dependent reflection coefficient, which produces changes in amplitude and phase of the reflected waves (Ravazzoli, 2001). Given that for the applications we are only considering viscous friction effects associated to Biot's global flow in homogeneously saturated porous media, which are negligible at low frequencies, the imaginary parts of the reflection coefficients are several orders of magnitude lower than the real parts. Consequently, in the numerical examples we only show their real part, hereafter denoted by R_{pp} for the P-wave and R_{ps} for converted shear waves.

To complete the model description, it is important to remark the assumption of no chemical interactions between the pore fluids and the frame, which allows us to employ a fluid substitution procedure to consider that the pore space is saturated by brine or oil and CO_2 in variable proportions. Variations of rock matrix elastic properties with effective pressure (related to the difference between confining and pore pressure), are not taken into account either. However, knowing the experimental effective pressure laws for the rocks under consideration would allow us to incorporate this effect in the computations (Ravazzoli, 2001).

3. Physical properties of CO_2 and reservoir fluids

We study the injection of a volume of carbon dioxide V_{CO_2} in a geologic reservoir in which the pore volume V_p at the pre-injection state is fully saturated by liquid reservoir fluids such as brine or oil, occupying a volume V_l. Then, we introduce the total *initial* CO_2 *saturation* S_{CO_2} and the liquid saturation S_l (corresponding to brine or oil), which satisfy the following relations:

$$S_{CO_2} = \frac{V_{CO_2}}{V_p}, \quad S_l = \frac{V_l}{V_p}, \quad \text{with } S_l + S_{CO_2} = 1. \tag{1}$$

According to Batzle and Wang (1992) and Carcione et al. (2006), part of V_{CO_2} is dissolved into the reservoir fluids and the remaining CO_2 takes the form of a free immiscible phase, giving rise to a two-phase fluid saturation. For simplicity, we leave out capillary pressure effects.

Since dissolution effects are negligible in brine (Batzle and Wang, 1992; Carcione et al., 2006), we only take this effect into account when the reservoir fluid is oil. In this case it is assumed that the CO_2-saturated oil behaves as a live oil whose physical properties can be obtained using Batzle and Wang (1992) empirical laws. With this idea and following the procedure presented by Carcione et al. (2006), we assume that the amount of CO_2 absorbed in an oil volume can be quantified using the gas-oil-ratio coefficient R_G in the form given by Batzle and Wang (1992), which represents the maximum volume ratio of liberated gas to remaining oil. Given that R_G corresponds to standard temperature and pressure conditions, an equivalent ratio R'_G at *in-situ* conditions is calculated through a mass balance. R'_G defines a critical saturation threshold S_c such that for $S_{CO_2} < S_c$ all CO_2 goes into solution in oil and there is no free CO_2 phase. For $S_{CO_2} \geq S_c$ the oil absorbs the maximum possible CO_2 and the rest gives rise to a free-CO_2 immiscible phase, with saturation denoted by $S^f_{CO_2}$. In this way, we can define the free CO_2 saturation S_g in the general form:

$$S_g = \begin{cases} 0 & \text{if } S_{CO_2} < S_c \\ S^f_{CO_2} & \text{if } S_{CO_2} \geq S_c, \end{cases} \tag{2}$$

being $S_l = 1 - S_g$ the liquid saturation. The *effective* physical properties of the oil-CO_2 mixture are then obtained by means of the following rules:

$$\text{mass density} \quad \rho^*_f = S_l\,\rho_l + S_g \rho_{CO_2} \quad \text{(weighted average)}, \tag{3}$$

$$\text{bulk modulus} \quad \frac{1}{K^*_f} = \frac{S_l}{K_l} + \frac{S_g}{K_{CO_2}} \quad \text{(isostress Reuss average)}, \tag{4}$$

$$\text{viscosity} \quad \eta^* \simeq \eta_{CO_2}\left(\frac{\eta_l}{\eta_{CO_2}}\right)^{S_l} \text{(Teja and Rice, 1981)}, \tag{5}$$

where ρ_l, ρ_{CO_2} are the individual liquid and CO_2 densities, η_l, η_{CO_2} their viscosities and K_l, K_{CO_2} the corresponding bulk moduli. Similar equations to (3), (4) and (5) hold for the CO_2-brine mixture using (1) with $S_g \equiv S_{CO_2}$.

The density, bulk modulus and viscosity of brine and live oil for the given *in-situ* temperature and pressure conditions are computed using the empirical relations given by Batzle and Wang (1992). For the computations we consider a typical brine salinity of 50,000 ppm. and a light oil with reference density equal to 0.78 gr/cm^3, equivalent to an API gravity equal to 50.

The corresponding properties of CO_2 (density and bulk modulus) for variable temperature and pressure can be computed using some of the general equations of state (EOS) developed for real gases such as van der Waals (1873) or Peng and Robinson (1976) (McCain, 1990), or some more specific such as Span and Wagner (1996) or Duan et al. (1992). Some of these EOS are implemented as on-line resources.[1]

To our knowledge, there is not a full agreement yet in geophysical literature about which EOS is the most appropriate to represent CO_2 properties at the temperatures and pressures found in geologic reservoirs. Then for our computations, we employ the fifteen-parameter EOS given by Duan et al. (1992), valid for pressures in the range 0–800 MPa and temperatures from 0 to 1000 °C, which guarantees a suitable representation of CO_2 properties at different states. In some cases, for comparison we also used the well known van der Waals (1873) cubic EOS.

To estimate CO_2 viscosity we used the formulas derived by Fenghour et al. (1998) from laboratory experiments, who found that CO_2 viscosity depends on both temperature and pressure. However it must be emphasized that for frequencies in the seismic range the influence of the effective viscosity in seismic velocities and reflection coefficients is minor.

Depending on the *in-situ* pressure and temperature conditions, CO_2 can exist in the subsurface in different phases (gas, liquid, supercritical and solid). We recall that the *critical point* for CO_2 occurs at a temperature $T_c = 31.1$ °C and a pressure $P_c = 7.39$ MPa. At temperatures higher than T_c and pressures higher than P_c, CO_2 is in a supercritical state, where it is compressible like a gas but with the density of a liquid. This important characteristic of CO_2 behavior is particularly relevant for its underground storage since supercritical CO_2 can fill the available pore volume with minimum buoyancy effects (Bachu, 2003). Temperatures and pressures near the critical point commonly occur in applications involving CO_2, such as enhanced oil recovery techniques and sequestration projects (Meadows, 2008). However, as pointed out by Bachu (2003), the depth at which CO_2 supercritical conditions are met is highly variable and strongly dependent on surface temperature and geothermal gradients, even within a single basin. In addition, the pressure regime of the basin (normal or abnormal), is also very important and is related to its geologic history, existence of sealing faults, permeability barriers and the occurrence of overpressure generation mechanisms (Osborne and Swarbrick, 1997).

4. Amplitude vs. angle analysis

Variations in the reflection coefficients with angle of incidence are commonly used in reservoir geophysics to infer properties about the lithology and fluid type of reservoir rocks (Avseth et al., 2005; Mavko et al., 1998). In this article, we investigate whether AVA coefficients can be usefully applied to the characterization of CO_2 accumulations, a problem of particular relevance for monitoring its migrations across permeable layers.

For the applications, we consider a 50 Hz plane P-wave striking the horizontal interface between a porous poorly consolidated sandstone, with high porosity and permeability, i.e. with good storage capacity, overlain by a shale layer acting as sealing rock. For the sandstone we consider the following parameters, taken from Dutta and Odé (1983): porosity 30%, permeability 1 Darcy, solid grain bulk modulus 35 GPa, frame bulk and shear moduli 1.7 GPa and 1.855 GPa and grain density 2.65 gr/cm^3. The corresponding properties of the upper shale layer are: porosity 25%, permeability 0.001 Darcy, solid grain bulk modulus 20 GPa, frame bulk and shear moduli 3.11 GPa and 1.528 GPa and grain density 2.45 gr/cm^3. The shale rock is assumed to be fully saturated with brine and the sandstone is assumed to be saturated by mixtures of brine and CO_2, in one case, and miscible mixtures of oil and CO_2 in another case, in variable volumetric proportions. The physical parameters of the fluids at the different physical states are shown in Table 1.

In the near offset domain or below the critical angle, we assumed that the R_{pp} reflection coefficient as a function of the incidence angle θ can be approximated in the usual form:

$$R_{pp}(\theta) \simeq A + B\,sin^2\theta + C\left(tan^2\theta - sin^2\theta\right), \tag{6}$$

where the coefficient A is the so called *intercept*, B the *gradient* (Castagna et al., 1998) and C the *curvature* (Barnola and White, 2001). The intercept is equal to the normal incidence reflection coefficient and is controlled by the contrast in acoustic impedance between both media. The gradient is more complex in terms of rock properties and is related to contrasts in density, in compressional and shear wave velocities (Avseth et al., 2005). The third parameter is important at far offsets and near critical angles (Mavko et al., 1998). Eq. (6) can be used to carry out a parametric analysis on the A, B and C coefficients to study their sensitivity at different saturation levels by implementing a standard fitting procedure on the results obtained for $R_{pp}(\theta)$.

With the aim of analyzing the behavior of the seismic reflectivity at different scenarios, in the following subsections we perform numerical experiments for variable CO_2 saturation, ranging from 0 to 100%, and different physical states (supercritical, gaseous and liquid), according to the location of the temperature and pressure pairs in the CO_2 phase diagram. A linear relationship between *in-situ* temperature and pressure can be obtained by assuming that the pore pressure at any depth z is hydrostatic, i.e. $P = \rho_w g z$, where ρ_w is formation water density and g the gravity constant. Also, considering a surface temperature T_0 and a geothermal gradient G, so that $T = T_0 + Gz$, it is straightforward that

$$P = \left(\frac{\rho_w g}{G}\right)(T - T_0). \tag{7}$$

Table 1
Physical properties of brine, oil and CO_2 at different physical states, according to Batzle and Wang (1992), Duan et al. (1992) and Fenghour et al. (1998). The live oil parameters correspond to the maximum CO_2 absorbed.

Physical State	CO_2	Brine	Saturated Live Oil
Gaseous CO_2	$K = 0.0049$ GPa	$K = 2.5986$ GPa	$K = 0.4978$ GPa
$T = 40$ °C	$\rho = 0.1498$ gr/cm^3	$\rho = 1.0287$ gr/cm^3	$\rho = 0.67$ gr/cm^3
$P = 6$ MPa	$\eta = 0.1787\ 10^{-3}$ Poise	$\eta = 0.785\ 10^{-2}$ Poise	$\eta = 0.0197$ Poise
Supercritical CO_2	$K = 0.01397$ GPa	$K = 2.6234$ GPa	$K = 0.2975$ GPa
$T = 40$ °C	$\rho = 0.6452$ gr/cm^3	$\rho = 1.0304$ gr/cm^3	$\rho = 0.60$ gr/cm^3
$P = 10$ MPa	$\eta = 0.4963\ 10^{-3}$ Poise	$\eta = 0.784910^{-2}$ Poise	$\eta = 0.0197$ Poise
Liquid CO_2	$K = 0.0931$ GPa	$K = 2.5009$ GPa	$K = 0.3283$ GPa
$T = 20$ °C	$\rho = 0.8535$ gr/cm^3	$\rho = 1.03607$ gr/cm^3	$\rho = 0.597$ gr/cm^3
$P = 10$ MPa	$\eta = 0.8089\ 10^{-3}$ Poise	$\eta = 0.01101$ Poise	$\eta = 0.0496$ Poise

[1] See for example the *Fluid Properties Explorer* of the Consortium for Research in Elastic Wave Exploration Seismology, Calgary University (CREWES) web page: http://www.crewes.org/ResearchLinks/ExplorerPrograms. Also The National Institute of Standards and Technology (NIST) *Chemistry WebBook*, http://webbook.nist.gov/chemistry/.

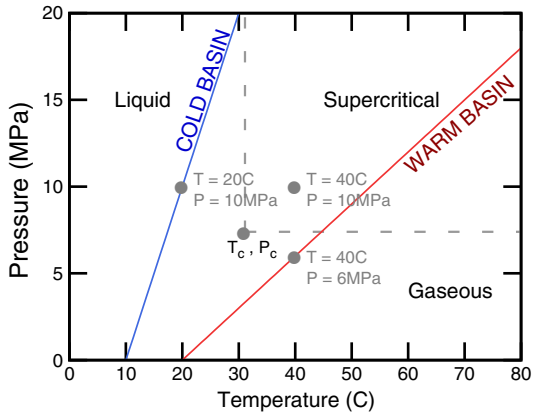

Fig. 1. Schematic Temperature vs. Pressure diagram and phase behavior of CO_2 (based on Fig. 3 of Bachu (2003)). The marked points indicate the temperature and pressure values used for the supercritical, gaseous and liquid state of CO_2 in the other figures. In addition, the position of the critical point (T_c, P_c) is also indicated.

According to (Bachu, 2003), we can distinguish *warm* basin conditions, where the trajectory in the P vs. T diagram is to the right of the critical point and goes through the gas and supercritical regions. The opposite geothermal conditions, defined as *cold*, are those in which the line P vs. T is to the left of the critical point (Fig. 1).

4.1. P-wave reflection curves at different physical states

The set of plots in Fig. 2(A)–(B), show the general behavior of R_{pp} as a function of incidence angle (from 0 to 90°), for the pre-injection case $S_{CO2}=0\%$ and for fixed saturation $S_{CO_2}=50\%$, for the three CO_2 states previously defined. Fig. 2(A) corresponds to CO_2-brine and Fig. 2(B) to CO_2-oil mixture, including dissolution effects in the latter case. Hereafter, according to the scheme in Fig. 1, for the gaseous state we consider a pore pressure $P=6$ MPa and a temperature $T=40$ °C, a condition that could be found within a warm basin at shallow depths (below 1 km). An intermediate situation, of great practical interest, is that of supercritical CO_2, which is analyzed by taking $P=10$ MPa and $T=40$ °C. We also consider the seismic reflectivity in the liquid region, by taking $P=10$ MPa and $T=20$ °C, a possible case in a cold basin at about 1 km depth. The pre-injection curve shown in Fig. 2 (A)–(B) corresponds to supercritical conditions. The pre-injection curves for gaseous and liquid states are very similar and are not shown for this reason.

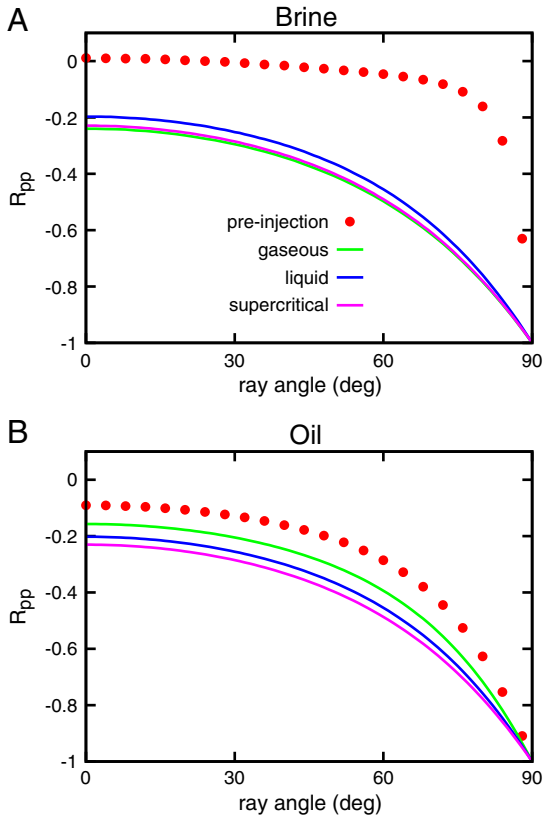

Fig. 2. Real part of the P-wave reflection coefficient vs. ray angle for $S_{CO_2}=50\%$ for (A) brine-CO_2 mixtures and (B) oil-CO_2 mixtures for: gaseous ($T=40$ °C, $P=6$ MPa), supercritical ($T=40$ °C, $P=10$ MPa) and liquid CO_2 ($T=20$ °C, $P=10$ MPa) conditions.

The set of curves in Fig. 2 show an AVA class III behavior, according to the standard AVA classification (Castagna et al., 1998). In particular, the plots corresponding to brine at supercritical state are similar to those recently published by Ghaderi and Landro (2009) for Utsira sandstone. As expected, due to the smaller impedance of the lower medium, we obtain a reflection coefficient with a negative real part for normal incidence, becoming more negative for higher angles. However, as will be evident later, for saturations lower than 5% a different AVA class can be found.

In the case of CO_2-brine mixture, the abrupt change in the reflection coefficient from the pre-injection to the post-injection state, is due to the contrast in physical properties and also because in this case, the CO_2 is a free phase (with no solubility effects). In the CO_2-oil case these variations are different, showing the influence of the dissolved CO_2 and the critical saturation on the acoustic properties of the live oil.

To analyze this effect in more detail, in Fig. 3 we show the behavior of the P-wave phase velocity for the CO_2-oil mixture vs. CO_2 saturation for the different temperature and pressure states. The corresponding critical saturations and gas-oil-ratios are: $S_c=61\%$, $R_G=125$ for the gaseous state, $S_c=40\%$, $R_G=232$ for the supercritical and $S_c=36\%$, $R_G=254$ for the liquid state. First, note that the differences in the velocities at the pre-injection state ($S_{CO_2}=0\%$) are due to the different temperature and pressure values of the reservoir oil. The sharp decrease in the wave velocity after S_c is associated to the existence of the free immiscible CO_2 phase, in agreement with the results found by Carcione et al. (2006). This is not observed for the liquid state due to the physical properties of the saturated oil and the high density of the liquid CO_2. Also, due to the lower absorption of CO_2 in oil at the temperature and pressure conditions for gaseous CO_2, for this state we observe a velocity higher than the other states. This results in a smaller reflection coefficient (in absolute value) as seen in Fig. 2(B). Moreover, given that R_{pp} is plotted at $S_{CO_2}=50\%$, the curves for the liquid and supercritical states are above the corresponding critical saturation, having a free CO_2 saturation. This results in smaller

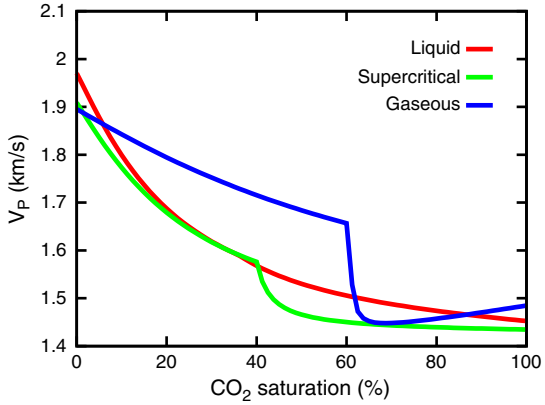

Fig. 3. P-wave phase velocity vs. saturation for CO_2-oil mixture at gaseous ($T=40$ °C, $P=6$ MPa), supercritical ($T=40$ °C, $P=10$ MPa) and liquid CO_2 ($T=20$ °C, $P=10$ MPa) conditions.

velocities and higher reflection coefficients than for the gaseous state, in which the critical saturation is above $S_{CO_2}=50\%$ and consequently, there is no free CO_2 phase for this particular experiment.

We conclude that, despite of the complex behavior due to the dissolution effects, which reduce the contrast in seismic reflectivity between pre-injection to post-injection states (compared to the CO_2-brine case), we observe that the discrimination of the *in-situ* CO_2 physical state may be more feasible in oil than in brine injection sites. The sensitivity of the P-wave reflection coefficient to CO_2 saturation will be studied in detail in Subsection 4.3 by analyzing the behavior of the corresponding AVA coefficients.

4.2. Influence of temperature and pressure

Considering the uncertainties in the *in-situ* formation, temperature and pore pressure, and to assess their influence on the seismic reflectivity, in Figs. 4 and 5 we plot the variations of R_{pp} with those state variables, assuming that they vary independently. We restricted to $\theta=30°$ and a limited number of CO_2 saturations steps (0%, 10%, 20%, 60% and 100%).

In Fig. 4 we show the model computations for a fixed supercritical pressure $P=10$ MPa, and temperatures ranging from 10 to 50 °C. In Fig. 4(A) we can see that for CO_2-brine fluids and for temperatures lower than 45 °C the reflection coefficient becomes more negative with increasing temperature. The most pronounced changes are observed for the minimum saturations.

In the case of CO_2-oil mixture, shown in Fig. 4(B), R_{pp} shows low sensitivity to temperature variations, except for high saturations. The jump between the 20% and 60% saturation curves is due to the passage through the critical saturations (for instance, recall that for $P=10$ MPa and $T=40$ °C, $S_c=40\%$), showing the increase in R_{pp} due to the presence of the free CO_2 phase.

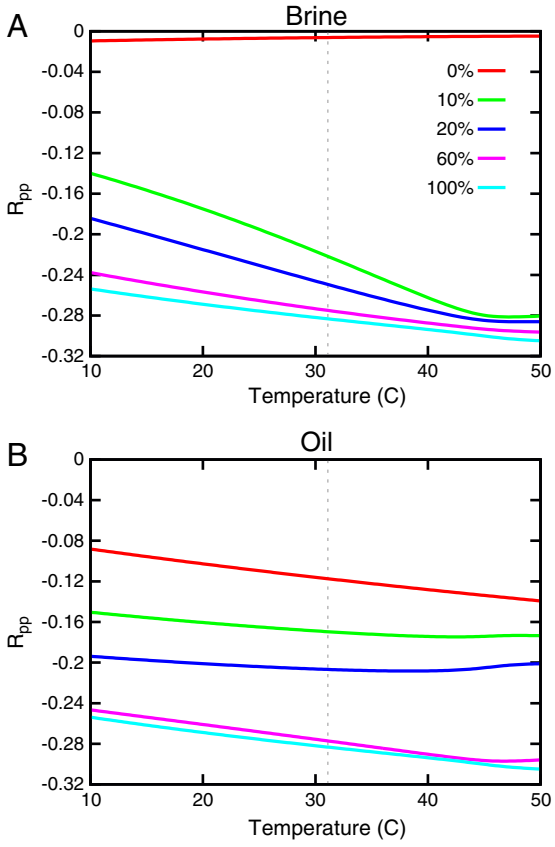

Fig. 4. Real part of the P-wave reflection coefficient vs. formation temperature for fixed pressure $P=10$ MPa and angle $\theta=30°$. The dotted vertical line denotes the critical temperature at $T_c=31.1$ °C.

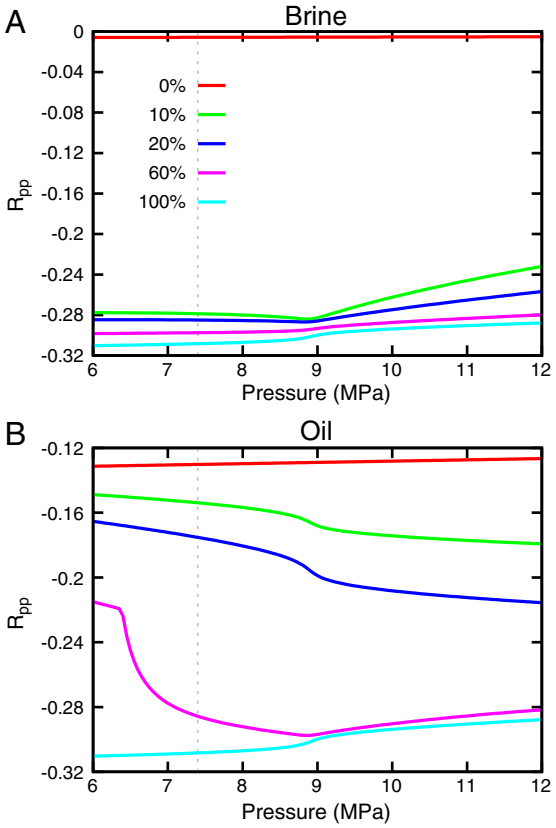

Fig. 5. Real part of the P-wave reflection coefficient vs. pore pressure for fixed temperature $T=40$ °C and angle $\theta=30°$. The dotted vertical line denotes the critical pressure at $P_c=7.39$ MPa.

The curves of R_{pp} vs. pressure for a supercritical temperature $T=40$ °C for CO_2-brine (Fig. 5(A)), show an almost constant behavior with pressure, with a noticeable change of trend at about 9 MPa, associated to the transition zone from gaseous to supercritical CO_2 for that temperature, an effect that was also corroborated using van der Waals (1873) EOS. Similar results were also found for normal incidence.

The behavior of R_{pp} vs. pressure in the case of CO_2-oil mixture, shown in Fig. 5(B), is very different, once again, due to the variable CO_2 dissolution in oil and the effect of the critical saturation. Nevertheless, the slight change in the transition zone from gaseous to supercritical CO_2 can still be observed.

From both Figs. 4 and 5 we observe that as CO_2 saturation increases, the effects of pressure and temperature are less marked. These results also clearly show the necessity of accurate estimations of pressure and temperature for a proper calibration of theoretical models and real time lapse seismic data, particularly at the early stages of injection, in which the errors could be significant.

4.3. AVA coefficients vs. partial CO_2 saturation at different conditions

In the next set of Figs. 6, 7 and 8, we plot the coefficients A,B,C to study their sensitivity at different saturation levels and physical states, by fitting Eq. (6) to the numerical results obtained for $R_{pp}(\theta)$.

For the case of CO_2-brine (dotted lines), we found that the intercept parameter A (Fig. 6), shows a monotonic decreasing behavior for the three physical states under consideration. These variations are more pronounced for CO_2 in liquid state, with significant percentage changes in the range from 5% to 40%. This is due to the behavior of the compressional velocity, which remains almost constant for CO_2 saturations greater than about 40%. In the

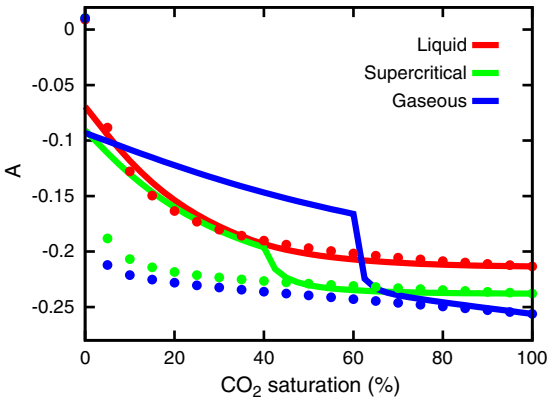

Fig. 6. Intercept (A) parameter vs. CO_2 saturation for brine-CO_2 mixtures (dotted lines) and oil-CO_2 mixtures (solid lines) at the different physical states.

same saturation range the variation of *A* for supercritical and gaseous CO_2 is much lower but still noticeable for the reservoir fluids considered. This allows us to clearly distinguish the liquid state from the gaseous and supercritical states.

The variations of *A* in the CO_2-oil mixture (solid lines) for saturations below the critical ones are pronounced for all states, being maximum for supercritical and gaseous states. The effects of dissolution of CO_2 in oil are responsible for such strong variations in this coefficient and in this case the gaseous state can be distinguished from the other two.

It is worthwhile to mention that for saturations lower than 5%, the intercept takes slightly negative values, consistent with an AVA Class II case.

Regarding the gradient *B* (Fig. 7) in CO_2-brine mixtures, it can be seen that it is always negative showing a trend similar to that of the intercept, except for the gaseous CO_2 state, in which a slightly opposite trend is observed. The most significant variations take place for CO_2 in liquid state, which can be useful to distinguish this particular state from the other two, with a gradient almost insensitive to saturation.

In the case of CO_2-oil saturation, slow and similar variations are observed below the critical saturations, being more pronounced for the liquid and supercritical states.

The curvature coefficient *C* (Fig. 8), compared with the *A* and *B* coefficients, is the least sensitive of the three, both, to the fluid type and saturation level of the injected CO_2 (note that to enhance the behavior of the curves the vertical axis of Fig. 8 is not the same as in Figs. 6 and 7). For both fluid types, we only found significant changes for CO_2 at the liquid state and for saturations in the range from 0 to about 40%. For higher saturations, the correct determination of such small changes may be strongly limited by the seismic resolution. In

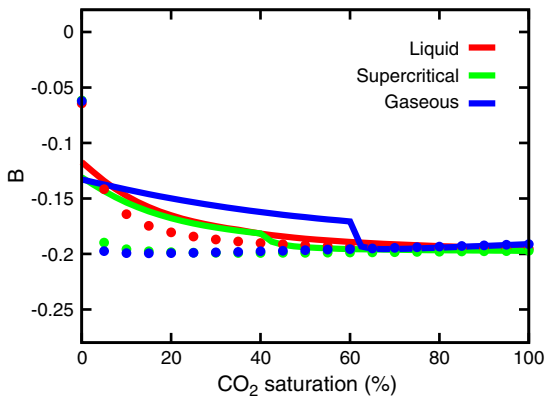

Fig. 7. Gradient (B) parameter vs. CO_2 saturation for brine-CO_2 mixtures (dotted lines) and oil-CO_2 mixtures (solid lines) at the different physical states.

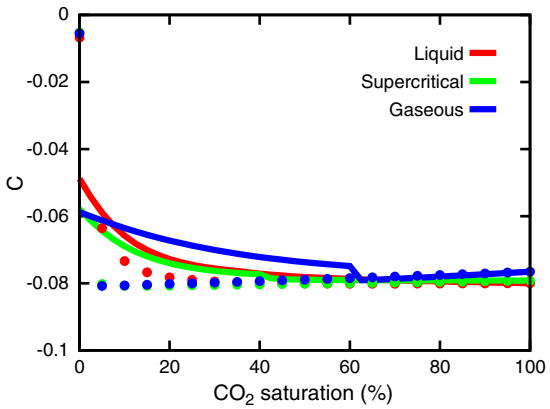

Fig. 8. Curvature (C) parameter vs. CO_2 saturation for brine-CO_2 mixtures (dotted lines) and oil-CO_2 mixtures (solid lines) at different physical states.

this sense, Brown et al. (2007) pointed out that AVA variations on the order of 5% are seismically detectable. Using this numerical threshold, we can state that variations in the parameter *C* do not contain much information with respect to these pore-fluid variations and consequently an AVO analysis based solely on *A* and *B* may be sufficient, being *A* the most sensitive for the determination of the CO_2 saturation state.

4.4. Effect of the EOS

In Fig. 9, we illustrate the coefficients *A* and *B* vs. CO_2 saturation, comparing the results obtained using van der Waals (1873) and Duan

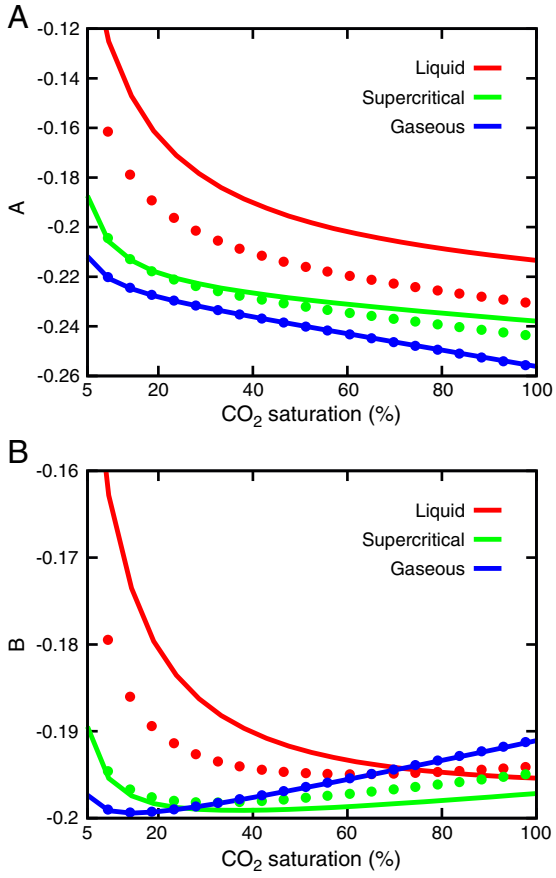

Fig. 9. A and B vs. CO_2 saturation for brine-CO_2 mixtures using Duan et al. (1992) (solid lines) and van der Waals (1873) (dotted lines) EOS at CO_2 supercritical conditions. To enhance the differences between the curves, saturations lower than 5% are not shown.

et al. (1992) equations of state. We only show the results corresponding to mixtures of CO_2 with brine at the three physical conditions, to observe the behavior of the EOS at the different states. We excluded from this figure CO_2 saturations lower than 5% to enhance the small discrepancies between the curves. From the results, we observe that for the supercritical and gaseous states, both EOS show an excellent agreement. The most important differences are observed for liquid CO_2 conditions, in which A and B may be underestimated when using van der Waals (1873) EOS. However this only affects the second decimal place. From these experiments we can conclude that, for seismic modeling applications, the choice of an EOS should not be a main concern since it does not change the results significantly.

4.5. Shear wave conversion

To conclude this work, we investigate whether shear wave reflections at the top of the CO_2 accumulation could be used for monitoring purposes. With this motivation, we modeled the shear wave reflection coefficient $R_{ps}(\theta)$ for mixtures of CO_2 with brine or oil at the different physical conditions under consideration. In Fig. 10(A)–(B) we show R_{ps} for angles in the range 0–90° for the case of gaseous CO_2 injected in brine and oil, respectively. Although the amount of energy conversion from compressional to shear wave mode is very low, we note that for this particular state R_{ps} at angles above 30 degrees is very sensitive to the CO_2 saturation degree in the case of CO_2-brine mixtures. This sensitivity is not observed when the reservoir fluid is oil, due to the solubility effects, which reduce the amount of free CO_2. However it can be useful as a rough indicator of the presence or absence of CO_2 in the reservoir oil.

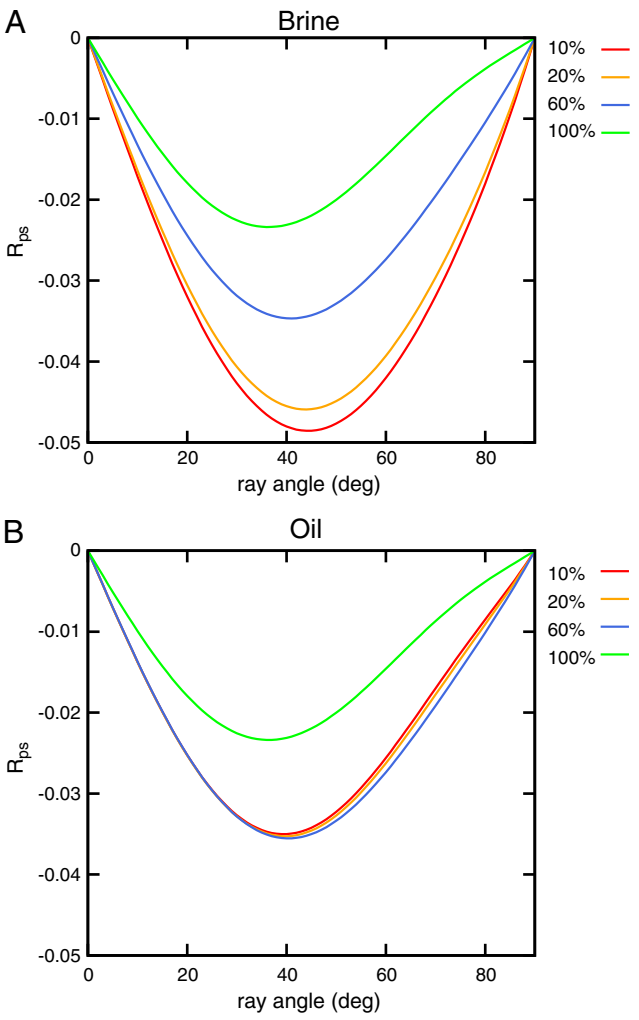

Fig. 10. Shear wave reflection coefficient vs. ray angle (A) for brine-CO_2 mixtures and (B) oil-CO_2 mixtures at gaseous CO_2 conditions ($T=40$ °C, $P=6$ MPa) for different fixed saturations.

5. Conclusions

We have analyzed the behavior of the compressional and shear wave reflection coefficients vs. angle of incidence at the top of a plane CO_2 accumulation within a poorly consolidated sandstone and beneath a shale caprock. Considering different temperatures and pore pressures corresponding to gaseous, supercritical and liquid CO_2 states, and using a standard three term R_{pp} approximation we have also modeled the variations of the AVA parameters A, B, C as a function of partial saturation for CO_2-brine and CO_2-oil mixtures.

In the particular case of CO_2 injected in oil reservoirs, the dissolution of variable fractions of CO_2 was taken into account in our model. Except for CO_2 at the liquid state, our model predicts a sharp decrease in the wave velocity for saturations higher than the critical, associated to the presence of a free CO_2 phase. This behavior is also clearly noted in the intercept A, being less pronounced in B and C.

The intercept and gradient parameters generally have a monotonic decreasing behavior, with a strong variation with respect to the pre-injection state. The most important percentage variations are always observed in the intercept, this parameter being the most sensitive to CO_2 saturation. In all cases analyzed, the coefficients A and B show significant changes for CO_2 saturations under about 40% or lower than the critical threshold. The curvature C does not bring much more information about saturation, since in most cases its variations are smaller than those observed in A and B. The lack of sensitivity of AVA parameters for very high saturations imposes a serious limitation to any attempt to quantify CO_2 saturation degree using AVA information.

In the particular case of oil reservoirs, our model estimates allows us to conclude that it would be possible to use time lapse seismic data to detect and monitor the free CO_2 phase, which forms after the oil is completely saturated. This is of particular interest in sequestration based in solubility trapping.

In some cases, reservoir temperature and pressure uncertainties can lead to significant errors in the modeled reflection coefficients, particularly at low CO_2 saturations. However, variations in AVA coefficients derived from implementing different equations of state for carbon dioxide are not significant.

With regards to the shear wave reflection coefficient at the top of the CO_2 accumulation, we found that the amount of energy conversion from compressional to shear waves is low but particularly sensitive to saturation for gaseous CO_2 injected in brine. Although this sensitivity is not observed when the reservoir fluid is oil, the analysis of shear wave mode conversions can be useful as a rough indicator of the presence or absence of CO_2 in the reservoir oil, which can be useful for monitoring purposes.

We also studied the sensitivity of the AVA coefficients to the thermodynamic conditions of the CO_2 at the subsurface. In the case of CO_2-brine mixtures it seems possible to discriminate a change in state from supercritical or gaseous to liquid (and vice versa), by analyzing the time lapse changes in A and B. For CO_2-oil mixtures this discrimination would be possible by means of the intercept, when the CO_2 changes to gaseous state. This suggests the possibility of using seismic reflection data to characterize the physical state of the CO_2 accumulated into brine or oil reservoirs, even with normal incidence data only. Moreover, the study of changes in AVA parameters over time may help to establish bounds on CO_2 saturation degree particularly at the early stages of accumulation below the caprock, assuming uniformly distributed CO_2.

The same kind of theoretical analysis can be performed for any other reservoir with a proper calibration of the rock physics model for

the CO_2 sequestration site. This can be useful to assess the applicability of the seismic reflection method for monitoring purposes.

Acknowledgements

The results presented here have been obtained in the CO2ReMoVe project, which envisages the development of technologies and procedures for monitoring and verifying geological CO_2 storage. The financial support of the European Commission and the industrial consortium involved is greatly appreciated.

Partial financing was also received from CONICET PIP 112-200801-00952 and by Agencia Nacional de Promoción Científica y Tecnológica PICT 03-13376. The authors thank William Harbert and an anonymous reviewer for their critical and accurate reviews of the original manuscript which was greatly improved by their comments. Also, to Dr. J. Germán Rubino for writing the code for CO_2 equations of state.

References

Avseth, P., Mukerji, T., Mavko, G., 2005. Quantitative Seismic Interpretation: applying Rock Physics Tools To Reduce Interpretation Risk. Cambridge University Press.

Arts, R.J., Eiken, O., Chadwick, R.A., Zweigel, P., van der Meer, L., Zinszner, B., 2004. Monitoring of CO_2 injected at Sleipner using time-lapse seismic data. Energy 29, 1383–1392.

Arts, R.J., Chadwick, R.A., Eiken, O., Trani, M., Dortland, S., 2007. Synthetic versus real time-lapse data at the Sleipner CO_2 injection site. Society of Exploration Geophysicists San Antonio Meeting, Expanded Abstracts, 26, pp. 2974–2978.

Bachu, S., 2003. Screening and ranking of sedimentary basins for sequestration of CO_2 in geological media in response to climate changes. Environmental Geology 44, 277–289.

Barnola, A.S., White, R.E., 2001. Gardner's relations and AVO inversion. First Break 19 (11), 607–611.

Batzle, M., Wang, Z., 1992. Seismic properties of pore fluids. Geophysics 57, 1396–1408.

Biot, M.A., 1956. Theory of propagation of elastic waves in a fluid-saturated porous solid. I. Low frequency range. Journal of the Acoustical Society of America 28, 168–171.

Biot, M.A., 1962. Mechanics of deformation and acoustic propagation in porous media. Journal of Applied Physics 33, 1482–1498.

Brown, S., Bussod, G., Hagin, P., 2007. AVO monitoring of CO_2 sequestration: a benchtop-modeling study. The Leading Edge 26 (12), 1576–1583.

Carcione, J.M., Picotti, S., Gei, D., Rossi, G., 2006. Physics and seismic modeling for monitoring CO_2 storage. Pure and Applied Geophysics 163, 175–207.

Castagna, J.P., Backus, M.M., 1993. Offset-dependent reflectivity-theory and practice of AVO analysis. Investigations in Geophysics, 8. Society of Exploration Geophysicists.

Castagna, J.P., Swan, H.W., Foster, D.J., 1998. Framework for AVO gradient and intercept interpretation. Geophysics 63, 948–956.

Chadwick, R.A., Arts, R., Eiken, O., 2005. 4D seismic quantification of a growing CO_2 plume at Sleipner, North Sea. In: Doré, A., Vinning, B. (Eds.), Petroleum Geology: NW Europe and Global Perspectives, Proceedings of the 6th Petroleum Geology Conference, pp. 1385–1399.

Deresiewicz, H., Rice, J.T., 1960. The effect of boundaries on wave propagation in liquid-filled porous solid: I. Reflection of plane waves at a true plane boundary. Bulletin of the Seismological Society of America 50, 599–607.

Duan, Z., Moller, N., Weare, J., 1992. An equation for the CH4-CO2-H2O system: I. Pure systems from 0 to 1000 C and 0 to 8000 bar. Geochimica et Cosmochimica Acta 56, 2605–2617.

Dutta, N., Odé, H., 1983. Seismic reflections from a gas-water contact. Geophysics 48, 148–162.

Gassmann, F., 1951. Über die elastizitat poroser Medien. Vierteljahrschrift der Naturforschenden Gesellschaft in Zurich 96, 1–23.

Ghaderi, A., Landro, M., 2009. Estimation of thickness and velocity changes of injected carbon dioxide layers from prestack time-lapse seismic data. Geophysics 74, O17–O28.

Hardage, B., Silva, D., 2009. Seismic steps aids sequestration, AAPG Explorer. http://www.aapg.org/explorer/2009/05may. May 2009.

IPCC Special Report on Carbon Dioxide Capture and Storage. In: Metz, B., Davidson, O., de Coninck, H.C., Loos, M., Meyer, L.A. (Eds.), Prepared by Working Group III of the Intergovernmental Panel on Climate Change. Cambridge University Press, Cambridge, United Kingdom and New York, NY, USA. 442 pp.

Mavko, G., Mukerji, T., Dvorkin, J., 1998. The Rock Physics Handbook: tools for Seismic Analysis of Porous Media. Cambridge University Press.

McCain Jr., W., 1990. The Properties of Petroleum Fluids. Penn Well Books, Tulsa, Oklahoma.

Meadows, M., 2008. Time-lapse seismic modeling and inversion of CO_2 saturation for storage and enhanced oil recovery. The Leading Edge 27 (4), 506–516.

Fenghour, A., Wakeman, W.A., Vesovic, V., 1998. The viscosity of Carbon Dioxide. Journal of Physical and Chemistry Reference Data 27 (1), 31–44.

Osborne, M.J., Swarbrick, R.E., 1997. Mechanisms for generating overpressure in sedimentary basins: a reevaluation. American Association of Petroleum Geologists Bulletin 81, 1023–1041.

Peng, D.Y., Robinson, D.B., 1976. A new two-constant equation of state. Industrial and Engineering Chemistry Fundamentals 15 (1), 59–64.

Purcell, C., Mur, A., Soong, Y., McLendon, T.R., Haljasmaa, I.V., Harbert, W., 2010. Integrating velocity measurements in a reservoir rock sample from the SACROC unit with an AVO proxy for subsurface supercritical CO_2. The Leading Edge 29 (2), 192–195.

Raistrick, M., 2008. Carbon capture and storage projects to challenge governments, scientists and engineers. First Break 26, 35–36.

Ravazzoli, C., 2001. Analysis of reflection and transmission coefficients in three-phase sandstone reservoirs. Journal of Computational Acoustics 9 (4), 1437–1454.

Santos, J.E., Corberó, J., Ravazzoli, C.L., Hensley, J., 1992. Reflection and transmission coefficients in fluid saturated porous media. Journal of the Acoustical Society of America 91, 1911–1923.

Span, R., Wagner, W., 1996. A new equation of state for carbon dioxide covering the fluid region from the triple-point temperature to 100 K at pressures up to 800 MPa. Journal of Physical and Chemical Reference Data 25, 1509–1596.

Teja, A.S., Rice, P., 1981. Generalized corresponding states method for viscosities of liquid mixtures. Industrial Engineering and Chemical Fundamentals 20, 77–81.

van der Waals, J.D., 1873. Over de continuiteit van den gas en vloeistoftoestand, dissertation, Leiden.